Mineralogy and mineral chemistry of oxide-facies manganese ores of the Postmasburg manganese field, South Africa

J. GUTZMER AND N. J. BEUKES

Department of Geology, Rand Afrikaans University, P.O. Box 524, Auckland Park, 2006, South Africa

Abstract

The diagenetic to very low-grade metamorphic manganese ores of the Postmasburg manganese field provide a unique example of oxide-facies manganese ores in a Palaeoproterozoic palaeokarst setting. The ores are composed mainly of braunite group minerals, including braunite, partridgeite and bixbyite, with rare braunite II and Ca-poor, silica-depleted braunite. Iron-poor partridgeite is distinguished from Fe-rich bixbyite and the occurrence of Ca-poor, silica-depleted braunite is reported for the first time. Braunite and partridgeite formed during early diagenesis but remained stable under greenschist facies metamorphic conditions. In contrast, bixbyite is apparently a product of metasomatic remobilisation under peak metamorphic conditions. It is suggested that local variations of the metamorphic mineral association reflect variations of the host rock composition and that they are not related to changing *P-T* conditions of metamorphic alteration, a model promoted by previous authors. The phase chemistry of braunite, braunite II and bixbyite is explained by the existing polysomatic stacking model for the braunite group. However, the chemical composition of partridgeite and Ca-poor, silica-depleted braunite can only be explained by introducing a distinct module layer, with partridgeite composition, to the existing polysomatic stacking model.

KEYWORDS: braunite, bixbyite, partridgeite, Campbellrand Subgroup, Transvaal Supergroup, manganese ore, Postmasburg, South Africa.

Introduction

THE manganese ores of the Postmasburg manganese field (Fig. 1A) are subdivided into ferruginous ores of the Western Belt and siliceous ores of the Eastern Belt (Fig. 1B). Ferruginous ores form most of the ore reserve and were mined extensively from 1922 to the late 1980s at Bishop, Lohatlha and Gloucester in the central part of the Western Belt (Fig. 1B). Siliceous ores occur locally in the Wolhaarkop Breccia and were mined on a small scale in a number of localities (Fig. 1B) (Hall, 1926; Nel, 1929; De Villiers, 1960).

Although the petrography of the manganese oxide ores of the Postmasburg manganese field has been studied in some detail (Schneiderhöhn, 1931; De Villiers, 1960, 1983; Plehwe-Leisen, 1985) very little is known about the chemical composition of the minerals. This is so because previous studies relied on the optical identification of ore and gangue minerals, a procedure unreliable for manganese oxides (Ramdohr and Frenzel, 1956; Frenzel, 1980). This paper describes the chemical composition of the various ore-forming minerals in greater detail and relates compositional variations to specific paragenetic and geological settings (Figs 1 and 2). Special attention is given to the crystal chemistry of the braunite group of minerals.

Analytical techniques

Identifications of ore and gangue minerals were based on a combination of X-ray powder diffraction analysis and ore petrographic studies. Electron microprobe analyses were carried out on a CAMECA CAMEBAX 355 microprobe with an aftached LINK ExLII energy dispersive spectrometer operated at 15 kV and 10 nA (on brass). Data acquisition was 80 sec per point analysis and all results were ZAF corrected. Several point analyses were performed for each mineral and average

Mineralogical Magazine, April 1997, Vol. 61, pp. 213–231

compositions determined to ensure the representative character of the results. Mineral formulae were calculated with Minfile, version 3-88 (Afifi and Essene, 1988).

Geological setting

The Postmasburg manganese field is situated on the Maremane dome (Fig. 1C) defined by dolomites of the Campbellrand Subgroup and iron-formation of the Asbestos Hills Subgroup of the early Palaeoproterozoic Transvaal Supergroup (Beukes, 1986; Grobbelaar and Beukes, 1986). Only the eastern half of this dome is exposed (Fig. 1C). To the west the Transvaal Supergroup is overlain unconformably by red beds of the Gamagara Formation of the late Palaeoproterozoic (2.2–1.9 Ga) Olifantshoek Group. Further to the west older rocks belonging to the Transvaal Supergroup, including iron-formation, diamictite and andesitic lavas, are thrust over the Gamagara Formation along the Black Ridge thrust fault (Fig. 1C) (Beukes and Smit, 1987).

Manganese ores, and closely associated hematitic iron ores (Grobbelaar and Beukes, 1986; Van Schalkwyk and Beukes, 1986) occur along or immediately below the pre-Gamagara unconformity. The iron ores, derived from hematitization of Asbestos Hills iron-formation, and its reworked equivalents in the Doornfontein conglomerate, are preserved as infills of large karstic sinkhole depressions (Van Wyk, 1980; Van Wyk and Beukes, 1982).

Siliceous manganese ores of the Eastern Belt are hosted by the Wolhaarkop chert breccia thought to represent a subsurface solution collapse breccia that accumulated as Asbestos Hills iron-formation slumped into karst depressions in the dolomite of the Campbellrand Subgroup (Fig. 3). Small lenses, pods, and sheet-like bodies of high-grade, siliceous manganese ore occur in the lower part of the Wolhaarkop breccia near the contact with the underlying dolomite (De Villiers, 1960). The braunite-rich ores are massive, fine to medium grained and dense.

Ferruginous ores of the Western Belt form the base of the Gamagara Formation in the central part of the Gamagara ridge where the succession unconformably overlies manganese-rich dolomite of the Reivilo Formation (Fig. 4). Aluminous shales or hematite pebble conglomerates of the Gamagara Formation rest conformably on the ferruginous manganese ore that is confined to karstic depressions in the Campbellrand dolomite. The conglomerates and shales were deposited in an alluvial floodplain environment (Van Schalkwyk and Beukes, 1986). The aluminous shales are composed of pyrophyllite, diaspore and kaolinite with variable amounts of hematite and minor amounts of illite, anatase and rutile. Some of the minerals present in the manganese shales and ores are listed in Table 1.

Fine and coarse-grained varieties of ferruginous manganese ores are present in the Western Belt. Fine grained bedded ores are composed of partridgeite, braunite, diaspore and ephesite (Fig. 2) and characterized by abundant sedimentary and diagenetic structures such as intercalations of shale or hematite pebble conglomerate, often showing contorted sedimentary bedding. In contrast, coarse grained ores have a vuggy or massive idioblastic appearance with abundant veining and brecciation. The coarse grained ores form irregular pods within the fine grained bedded ores and differ from the latter in that they contain abundant coarse grained iron-rich bixbyite in association with very coarse grained diaspore and ephesite (Fig. 2).

The geological setting of the manganese deposits strongly suggests accumulation as residual palaeo-

TABLE 1. List of some minerals encountered in the Postmasburg manganese field

Mineral Name	Formula
jacobsite	$Mn^{2+}Fe_2O_4$
hausmannite	$Mn^{2+}Mn_2^{3+}O_4$
braunite	$Mn^{2+}Mn_6^{3+}SiO_{12}$
partridgeite*	Mn_2O_3
bixbyite	α-$(Mn,Fe)_2O_3$
manganite	γ-MnOOH
romanèchite	$Ba_{1-2}Mn_8^{4+}O_{16}\cdot xH_2O$
cryptomelane	$K_{1-2}Mn_8^{4+}O_{16}\cdot xH_2O$
manganomelane**	$(Na,K,Ba)_{1-2}Mn_8^{4+}O_{16}\cdot xH_2O$
lithiophorite	$Li_2Mn^{2+}Mn_5^{4+}Al_4O_{18}\cdot 6H_2O$
pyrolusite	β-MnO_2
ramsdellite	MnO_2
diaspore	α-AlOOH
gamagarite	$Ba_2(Fe^{3+},Mn)[(OH,H_2O)/(VO_4)_2]$
ephesite	$(Na,Ca)Al_2[(OH)_2/Al(Al,Si)Si_2O_{10}]$
amesite	$(Mg,Fe)_2Al_2[(OH)_8/(Si_2,Al_2)O_{10}]$

* Partridgeite is not a mineral recognized by the IMA (International Mineralogical Association), see discussion in text.

** Following the suggestion by Frenzel (1980) the complex group of minerals with the generalized formula $A_{1-2}Mn_8^{4+}O_{16}\cdot xH_2O$ (A = Na,K,Pb,Ba) is in this study referred to as the manganomelane group. Several compositional end-members are distinguished in this group namely manjiroite (Na-rich), cryptomelane (K-rich), coronadite (Pb-rich) and romanèchite (Ba-rich). Phases of intermediate composition are referred to as manganomelane.

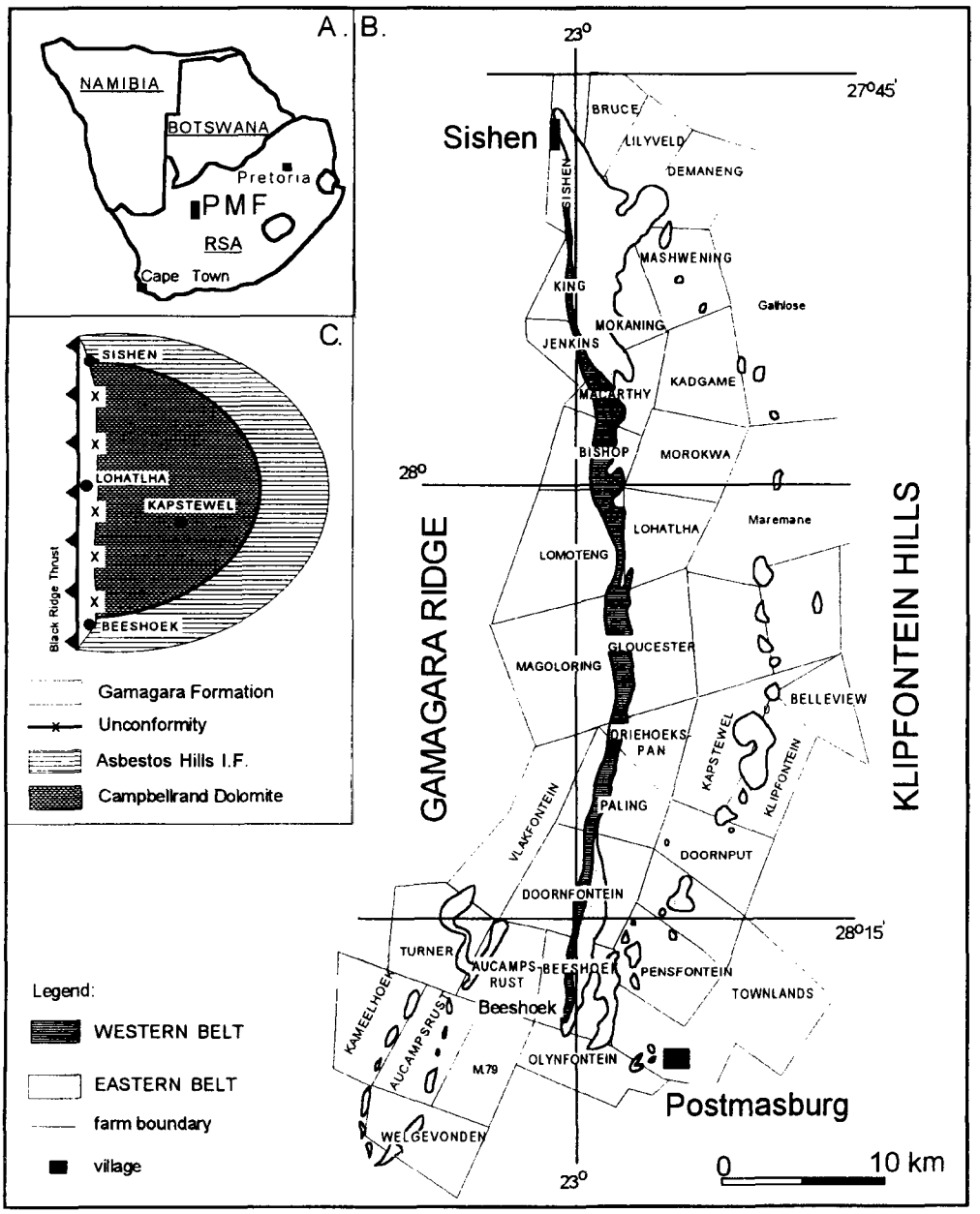

FIG. 1. Regional map of the Postmasburg manganese field showing the location of the deposits of ferruginous manganese ore along the Gamagara Ridge (Western Belt) and the occurrence of Wolhaarkop Breccia (and associated manganese ores of the siliceous type) in the Klipfontein Hills (Eastern Belt), the Gamagara Ridge and in the Aucampsrust area (modified after De Villiers, 1960).

karst sediments during the period of intensive weathering that preceded the deposition of the sediments of the late Palaeoproterozoic Olifantshoek Group (Grobbelaar and Beukes, 1986). The karstic manganese and iron-rich dolomites of the Campbellrand Subgroup not only host, but apparently

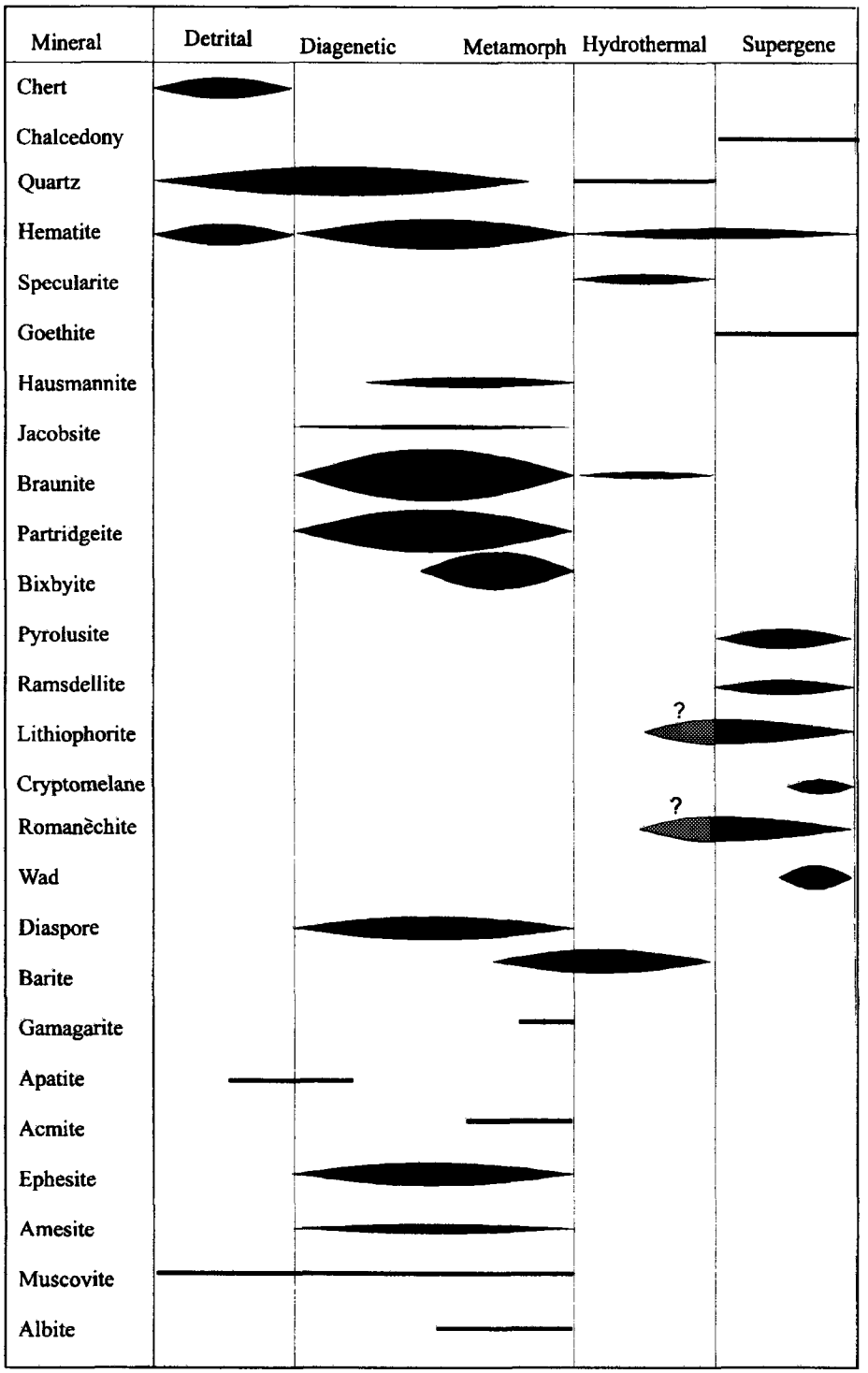

FIG. 2. Mineral paragenetic table for the manganese ores of the Postmasburg manganese field (after Gutzmer, 1996).

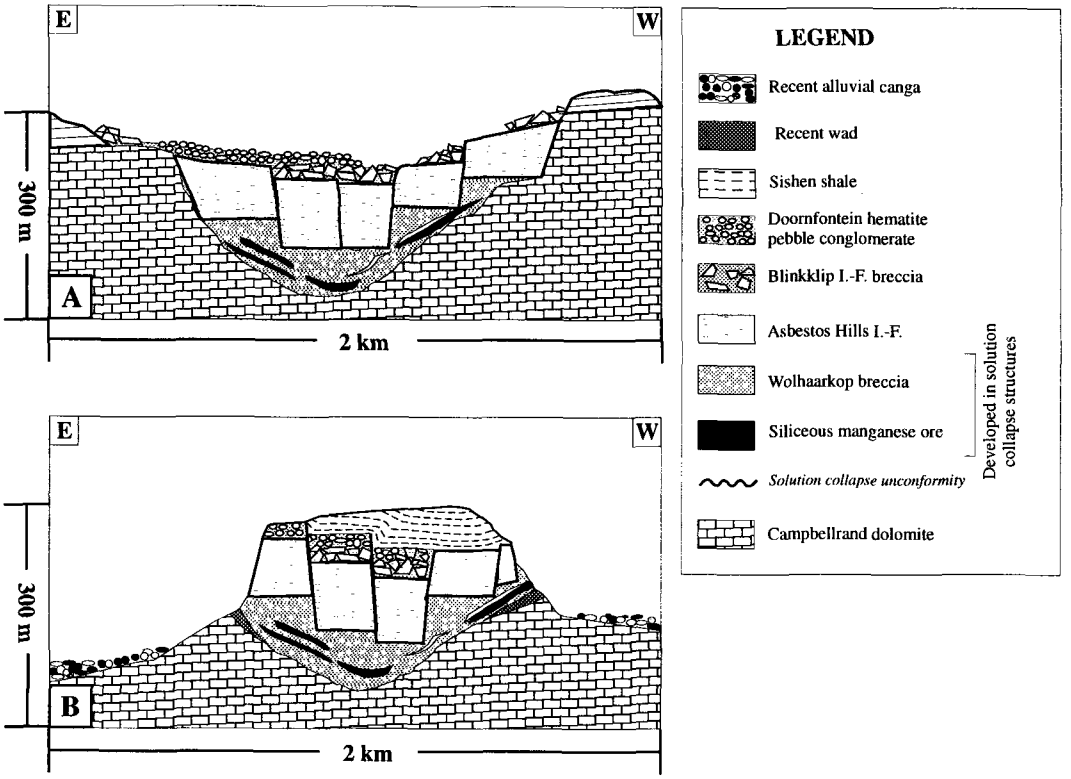

FIG. 3. Model for the origin of the Wolhaarkop Breccia and associated siliceous manganese ore of the Eastern Belt. (A) Wolhaarkop chert breccia accumulates as residual sediment in karst caves into which portions of hematitized Manganore Iron-Formation subsequently slump. Fluvial conglomerates of reworked iron-formation cover the slumped iron-formation. (B) Following burial and greenschist facies metamorphism, renewed terrestrial exposure and erosion lead to relief inversion. The sinkhole infills are positively exposed against the surrounding dolomite host. Alluvial canga deposits accumulate along the footslope of the hills (modified after Gutzmer, 1996).

also sourced the manganese deposits (Grobbelaar and Beukes, 1986). Indications are that siliceous manganese ores of the Eastern Belt accumulated in karst caves intimately associated with the Wolhaarkop subsurface solution collapse breccia (Fig. 3). In contrast, ferruginous manganese ores of the Western Belt were deposited together with lateritic clays (lower aluminous shales of the Gamagara Formation) in subaerial sinkhole depressions (Fig. 4).

Postmetamorphic lenses and veins of low temperature hydrothermal baryte and coarse grained specularite crosscut the manganese orebodies (Fig. 2). Subaerial exposure in geologically recent times resulted in relief inversion and positive weathering of manganese and iron-ore bodies against the surrounding dolomites (Figs. 3 and 4). Supergene manganese oxides such as romanèchite, cryptomelane, lithiophorite and pyrolusite formed at this time (Fig. 2).

Petrography

The siliceous manganese ores, situated in the Wolhaarkop chert breccia (Fig. 3), are composed of braunite, with minor amounts of partridgeite, hematite, authigenic quartz and recrystallized chert fragments (Fig. 5A). The latter were apparently derived from the dissolution of underlying dolomite (De Villiers, 1960). Braunite occurs as equigranular mosaic-textured aggregates composed of subhedral grains 5 to 1000 μm in diameter. Braunite crystals often show distinct concentric colour zonation from brown to brownish-grey (Fig. 5B). Lamellar and spotty intergrowth of different braunite varieties and of braunite with partridgeite are present. Needle-shaped and platy, anhedral grains of hematite are associated with braunite–partridgeite aggregates. Rare prismatic apatite crystals with a diameter of up to 250 μm (De Villiers, 1945*a*) are present and

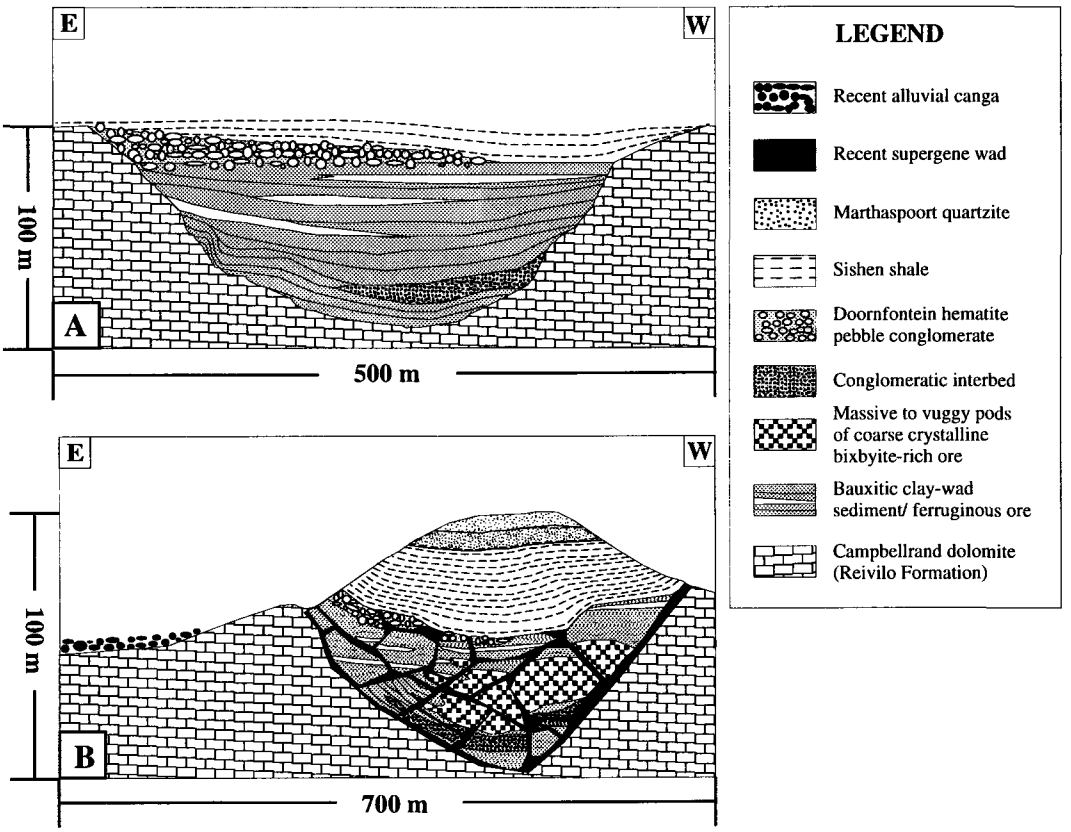

FIG. 4. Model for the origin of the ferruginous manganese ores of the Western Belt. (A) A layered succession of mixed bauxitic clay-ferromanganiferous wad with interbedded clay lenses and conglomeratic beds is deposited in open karst depressions of the Reivilo Formation and buried below hematite conglomerates and lateritic clays of the Gamagara Formation. (B) Greenschist facies metamorphism is succeeded by terrestrial exposure and erosion resulting in renewed karstification, brecciation of the manganese orebody, formation of romanèchite crusts and manganese wad and accumulation of alluvial canga deposits (modified after Gutzmer, 1996).

known to be replaced by braunite. Sheaf-like aggregates of Ba-muscovite occur in supergene altered siliceous ore. Coarse grained baryte occurs in irregular patches in the Wolhaarkop breccia and encloses large euhedral braunite crystals. Aggregates of needle-shaped acmite and compact crystalline masses of coarse grained albite are present in braunitic ores from Sishen and Mokaning (De Villiers, 1945*a*).

The Wolhaarkop breccia, which hosts the siliceous ores, is composed of recrystallized chert fragments set in a fine grained matrix of braunite, hematite and authigenic euhedral quartz. Many of the recrystallized chert fragments are overgrown by authigenic quartz, partly replaced by fine grained braunite. In contrast small authigenic quartz crystals developed in the braunite matrix of the breccia display no evidence of replacement by braunite (Fig. 5A).

The fine grained bedded ferruginous manganese ores of the Western Belt are composed of braunite, partridgeite, hematite and diaspore, with variable amounts of ephesite and amesite. Braunite is intimately intergrown with ephesite and amesite, whereas partridgeite is more abundant in oxide and diaspore-rich beds. Finely laminated and massive beds are present in the fine grained ore. Early diagenetic structures include ovoidal microconcretions (Fig. 5C), botryoidal layered crusts and anastomosing veinlets, all composed of braunite and/or partridgeite. Fine laminae are defined by slightly differing concentrations of braunite or partridgeite, grain size and/or degrees of supergene

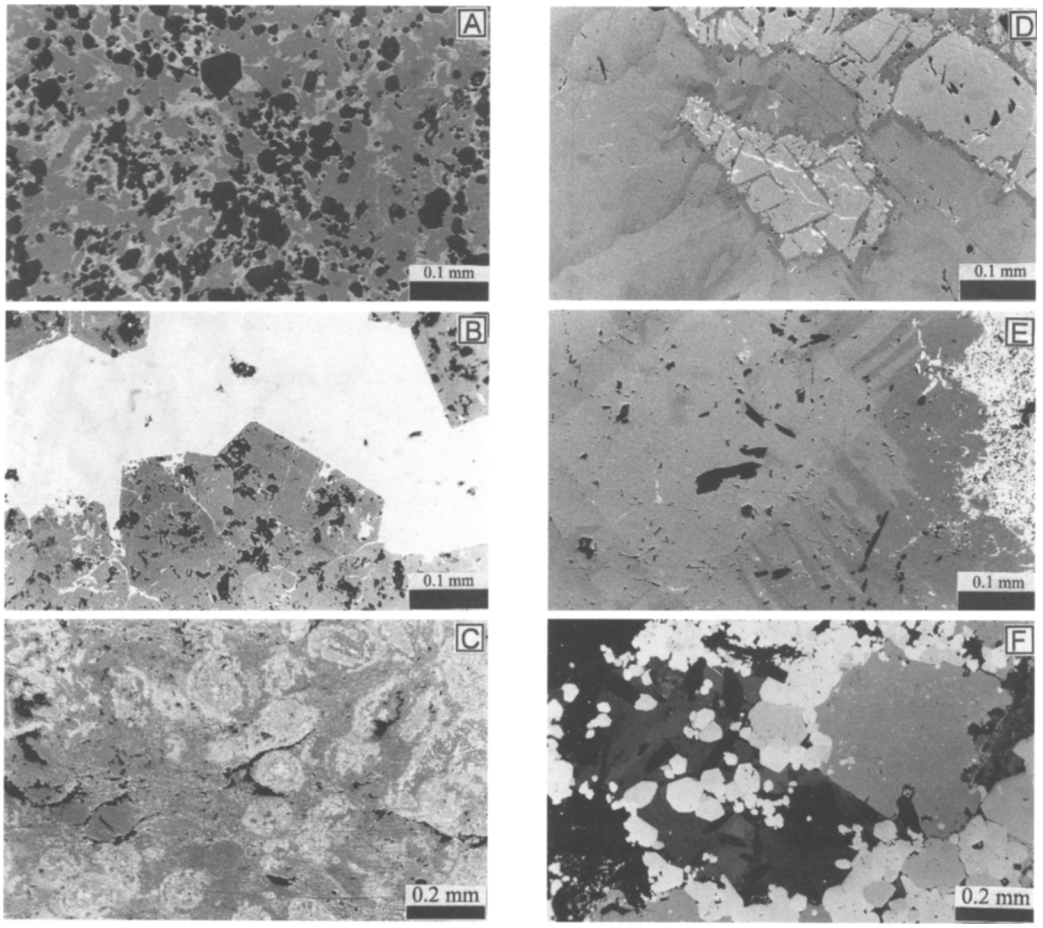

FIG. 5. Reflected light photomicrographs. (A) Small, authigenic quartz crystals in mosaic textured braunite matrix. Braunite is replaced along grain boundaries by supergene manganomelane (white) (oil immersion, MAN238); (B) Concentrically zoned euhedral braunite crystals in vug filled by supergene romanèchite (white) (oil immersion, BEE208); (C) Diagenetic partridgeite microconcretions (light grey) that are partly replaced by supergene romanèchite (white) in a massive braunite matrix (grey) (oil immersion, GLO187); (D) Braunite lamellae (grey) intersect partridgeite grain (light-grey), in a matrix of finely intergrown Si-depleted braunite and braunite. Partridgeite and Si-depleted braunite are replaced by romanèchite (white) (oil immersion, GLO187); (E) Flame structures of Si-depleted braunite (medium grey) extending from the surface of a large partridgeite grain (light grey) into braunite (grey). Romanèchite appears white, diaspore black (oil immersion, GLO187); (F) Large cubes of bixbyite (light grey) with small hematite inclusions (white) surrounded by hematite (white), lithiophorite (dark grey) and diaspore (black, short laths) (oil immersion, LOH79).

alteration. Massive beds are composed of aggregates of braunite with well developed equigranular mosaic texture and massive to idioblastic partridgeite. Intimate intergrowths of braunite with partridgeite are common (Fig. 5D). In one sample from Glosam mine, flame-shaped intergrowths of Ca-poor silica-deplete braunite protrude from partridgeite–braunite grain boundaries into the surrounding braunite (Fig. 5E). Small anhedral hausmannite grains occasionally replace partridgeite. Ephesite and diaspore occur as gangue minerals. Micaceous ephesite plates, up to 100 μm long, and up to 500 μm long diaspore laths define distinct laminae or irregular clusters.

The coarse grained ferruginous manganese ores of the Western Belt are composed of cubic bixbyite idioblasts that are up to 30 mm in diameter. The bixbyite crystals are intimately intergrown with coarse grained diaspore, ephesite, and amesite (Fig. 5F), mosaic-textured aggregates of braunite and rare plates of hematite. Bixbyite cubes are characterized by lamellar twinning (Schneiderhöhn, 1931; Ramdohr, 1969) and concentric growth zonation along {100}. Oriented intergrowth inclusions (Ramdohr, 1969) of thin braunite and braunite II lamellae (De Villiers, 1992) (10 to 100 μm long) and up to 100 μm long diaspore laths appear along {100} and {111}, illustrating the cogenetic formation of these minerals with bixbyite. Gamagarite, in a unique occurrence from Glosam mine, occurs as clusters of needle-shaped crystals (up to 1 cm long) in bixbyite-rich ore (De Villiers, 1943*b*).

Supergene ores are mainly composed of manganomelane group minerals (Frenzel, 1980). Romanèchite, cryptomelane and manganomelane of intermediate composition replace partridgeite, braunite and bixbyite (Fig. 6A). Lithiophorite is abundant in the ferruginous manganese ores as replacement product of diaspore and ephesite (Figs. 6B and C). Minor amounts of manganite, pyrolusite, ramsdellite, goethite, and X-ray amorphous wad occur as products of supergene alteration. Pyrolusite is common as vug or vein fill in some of the supergene ores especially (Fig. 6D). Some ramsdellite is also present in the supergene ores and may be easily mistaken with pyrolusite (Plehwe-Leisen, 1985).

Mineral chemistry

Braunite. Three compositionally distinct varieties of braunite occur in the Postmasburg manganese ores, namely braunite, braunite II, and Ca-poor silica-depleted braunite. Major element electron microprobe analyses of braunite *sensu stricto* (from now on simply called braunite) indicates a generally Fe-poor composition with a stoichiometric SiO_2 content close to 10 wt.% (Table 2) and the formula $(Mn^{2+}_{0.7-1}Ca^{2+}_{0-0.2})(Mn^{3+}_{5.5-5.9}Al_{0-0.2}Fe^{3+}_{0-0.4})(Si_{0.9-1.1}Ti_{0-0.1})O_{12}$. The contents of Fe, Ti, and Ca are apparently controlled by the coexisting mineral

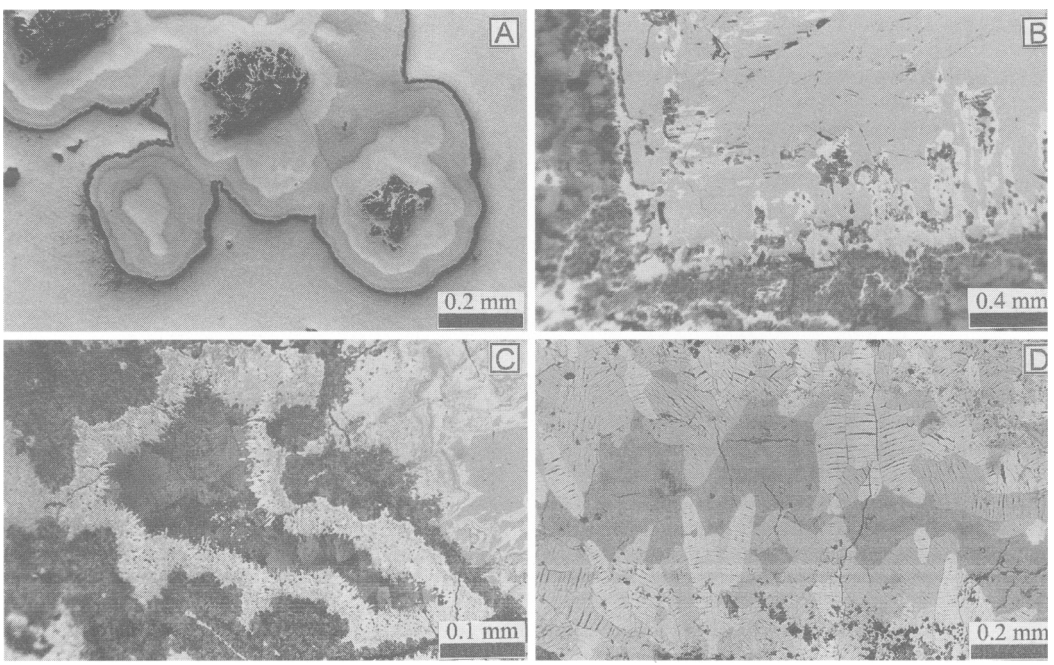

FIG. 6. Reflected light photomicrographs (A) Botryoidal romanèchite (BIS244). (B) Large bixbyite cube replaced by fine crystalline romanèchite (white) and lithiophorite (dark grey) (LOH79); (C) Close up of previous photograph. Note that different generations of manganomelane/romanèchite are characterized by different colour shades. Note also polishing scratches and strong bireflectivity on coarse crystalline lithiophorite (oil immersion); (D) Coarse crystalline supergene pyrolusite fills in vugs in braunitic manganese ore BEE210).

assemblage. Braunite in close association with hematite contains 2.51 and 5.41 wt.% Fe_2O_3 whereas braunite in assemblages devoid of hematite contains between 0.1 and 2.21 wt.% Fe_2O_3. Concentrations of TiO_2 vary between 0.41 and 1.05 wt.% TiO_2 in braunite associated with aluminous shales, but are less than 0.1 wt.% TiO_2 (Table 2, Fig. 7) in braunite from ferruginous and siliceous manganese ores. SiO_2 contents decrease with increasing TiO_2 contents, strongly suggesting substitution of Si by Ti (Table 2). CaO appears to be enriched in braunite in ferruginous manganese ores (1.85–3.09 wt.% CaO), as compared with braunite hosted by aluminous shales (0.3–0.54 wt.% CaO) and siliceous manganese ores (0.70–1.62 wt.% CaO). Al_2O_3 contents are apparently independent of the coexisting mineral assemblage (Table 2).

Braunite II (a variety of braunite containing only 3–5 wt.% SiO_2, a similar amount of CaO and about 20 wt.% Fe_2O_3) was first described from the Kalahari manganese field (De Villiers, 1945*a*; De Villiers and Herbstein, 1967). De Villiers (1992) described lamellar braunite II that contains 4.8 wt.% SiO_2, 12 wt.% Fe_2O_3 and 4.64 wt.% CaO as inclusions in bixbyite from Glosam mine in the Postmasburg manganese field. Rare flame-shaped growths of another variety of braunite, i.e. Ca-poor silica-depleted braunite (Figs. 5D and 5E), contain as little as 1.1 wt.% CaO, between 3.3 and 4.2 wt.% SiO_2, and 0–3.54 wt.% Fe_2O_3, but high concentrations of Al_2O_3 (2.71–3.99 wt.%) (Table 2). Analytical totals of Ca-poor silica-depleted braunite add up to somewhat more than 100 wt.%. This suggests that some of the manganese may be present as MnO and not as Mn_2O_3. This is in contrast to braunite II in which the divalent cation position is entirely occupied by Ca (De Villiers and Buseck, 1989). The compositional data of the Ca-poor silica-depleted braunite lead to the formula $Ca_{0.1}Mn^{3+}_{6.8}Fe^{3+}_{0.1}Al_{0.5}Si_{0.4}O_{12}$.

Bixbyite and partridgeite. Iron-poor partridgeite, containing less than 5 wt.% Fe_2O_3, and iron-rich bixbyite, containing 10 to 22 wt.% Fe_2O_3, are present. Partridgeite was described by De Villiers (1943*a*) as a new mineral species from the Postmasburg manganese field. However, Mason (1944) and Roy (1981) challenged the significance of the name partridgeite and it became custom to refer to it as iron-poor bixbyite (Plehwe-Leisen, 1985; Roy *et al.*, 1990). During this study abundant partridgeite was examined microscopically and compared with associated iron-rich bixbyite. The two phases are easily distinguished. Similar to the descriptions by De Villiers (1943*a*) and De Villiers (1960), partridgeite appears anisotropic whereas bixbyite is isotropic. Microprobe analyses confirmed that those grains identified optically as partridgeite are in fact iron-poor and contain less than 5 wt.% Fe_2O_3 whereas examples of bixbyite

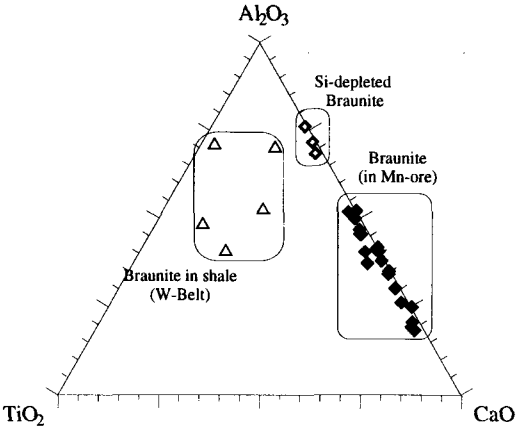

FIG. 7. Triangular diagram Al_2O_3–TiO_2–CaO to distinguish braunite formed in different geological environments.

consistently contain more than 10 wt.% Fe_2O_3 (Table 3). The mineral name partridgeite is therefore retained in this study to distinguish iron-poor anisotropic α-Mn_2O_3 from iron-rich isotropic bixbyite. Chemical formulae of $(Mn^{3+}_{1.90-1.96}Al_{0.02-0.05}Fe^{3+}_{0.01-0.04})O_3$ for partridgeite and $(Mn^{3+}_{1.52-1.64}, Fe^{3+}_{0.24-0.37}, Al_{0.05-0.09})O_3$ for bixbyite are derived from the microprobe data (Table 3).

The minor element composition of partridgeite and bixbyite is very similar. MgO, CaO, BaO and alkali contents are well below 0.5 wt.% (Table 3). Al_2O_3 concentrations vary between 0.45 and 2.80 wt.% in partridgeite (Table 3) and appear on average a little larger in bixbyite (1.41–2.90 wt.%) (Table 3). This is also true for TiO_2 with partridgeite containing less than 0.15 wt.% TiO_2 and bixbyite containing between 0.06 and 0.68 wt.% TiO_2.

Hausmannite. Microprobe analyses of hausmannite were impeded by the fact that it is virtually always replaced by supergene romanèchite. Only one sample with sufficiently fresh hausmannite was encountered (Table 3). Minor element contents of hausmannite are low and within the range reported in the literature (Frenzel, 1980; Roy, 1981). Al^{3+} and Fe^{3+} are likely to substitute for Mn^{3+} in the hausmannite structure, suggesting a formula of $Mn^{2+}_{1.05}(Mn^{3+}_{1.8}Al^{3+}_{0.1}Fe^{3+}_{0.05})O_4$.

Manganomelane group and pyrolusite. The Ba-rich member of the manganomelane group, romanèchite, contains between 13.3 and 15.6 wt.% BaO, less than 1 wt.% Na_2O and K_2O and less than 0.5 wt.% MgO, CaO and SiO_2 (Table 4). The Fe_2O_3 and Al_2O_3 contents are below 2 wt.%. Cryptomelane contains significantly more K_2O (4.92–5.42 wt.%) than BaO (0.43–1.99 wt.%) or Na_2O (0.18–0.45

TABLE 2. Composition of braunite and Si-depleted braunite in different ores of the Postmasburg manganese field (selected analyses, data in wt.%)

Sample No.	AUC198.2	BEE213	BEE214	DO169	KAP230	MAN238	GLO185.1	LOH179	GLO185.1	GLO185.3	GLO187	LOH176
Mineral	Br	Br	Br	Br	Br	Br	Br	Br	Si-Br	Si-Br	Br	Br
Host	siliceous manganese ore						ferruginous manganese ore				shale	
N	4	5	10	3	7	6	8	10	10	10	3	5
SiO_2	10.3	10.5	10.3	10.8	10.6	10.7	10.6	10.0	4.19	4.07	9.78	9.10
TiO_2	0.05	0.1	0.04	LLD	LLD	0.02	0.01	0.09	0.04	0.05	0.98	1.05
Al_2O_3	0.35	0.50	1.27	0.80	1.41	0.51	1.27	0.58	3.99	3.03	1.06	1.28
Fe_2O_3	0.34	5.00	2.51	1.80	0.16	4.58	0.06	0.42	LLD	3.54	4.19	2.87
Mn_2O_3	78.6	72.4	75.4	75.7	76.9	72.7	78.4	76.7	92.2	89.8	71.4	73.0
MnO*	8.58	11.1	9.07	9.80	9.38	10.5	7.98	11.8	n.c.	n.c.	10.8	12.4
MgO	LLD	LLD	LLD	0.10	0.13	LLD	LLD	0.15	0.10	LLD	0.20	LLD
CaO	1.52	0.70	1.24	1.20	1.30	0.96	1.85	0.15	1.21	1.16	0.54	0.30
BaO	0.24	0.06	0.12	0.10	0.13	0.05	0.06	0.05	0.06	0.07	0.27	0.04
Na_2O	LLD	LLD	0.17	0.10	LLD	0.15	LLD	0.15	0.13	0.10	0.17	LLD
K_2O	LLD	LLD	LLD	LLD	LLD	LLD	LLD	LLD	LLD	LLD	0.59	LLD
Total	100.1	100.4	100.2	100.4	100.1	100.2	100.4	100.1	102.0	101.9	100.0	100.2
Mn/(Mn+Fe)	1.00	0.94	0.97	0.98	1.00	0.95	1.00	1.00	1.00	0.96	0.95	0.97

Abbreviations: N - number of analyses; LLD - lower than detection limit; Br-braunite; Si-Br- silica-depleted braunite; * Mn^{2+}-Mn^{3+} charge balance calculated, n.c. - charge balance not calculated.

TABLE 3. Composition of partridgeite, bixbyite and hausmannite in different ores of the Postmasburg manganese field (selected analyses, all data in wt.%)

Sample No.	BEE214.1	BEE214.2	DO161	PAL219.4	GLO185.3	GLO193	LOH179	BIS241	BIS243	PAL219.3	PAL228.1	PAL228.2	PAL219
Mineral	Ptr	Ptr	Ptr	Ptr	Ptr	Ptr	Ptr	Bx	Bx	Bx	Bx	Bx	Hs
Host	siliceous manganese ore			ferruginous manganese ore									
N	5	5	3	2	5	3	10	10	3	5	9	4	9
SiO_2	0.95	0.50	0.57	0.65	0.28	0.69	0.78	0.14	0.13	1.48	0.48	0.45	0.25
TiO_2	LLD	0.04	0.05	0.05	0.02	0.13	0.09	0.45	0.37	0.16	0.55	0.58	0.07
Al_2O_3	0.54	0.99	0.45	1.25	0.61	1.12	1.55	2.89	1.88	1.97	1.58	1.80	1.51
Fe_2O_3	0.40	0.04	0.24	1.90	0.67	0.54	1.15	13.9	20.5	12.4	18.6	18.8	1.07
Mn_2O_3*	98.0	98.5	98.7	96.7	98.6	97.5	95.3	82.6	76.4	84.0	78.6	78.4	63.34
MnO													33.43
MgO	0.06	0.04	LLD	0.20	LLD	LLD	LLD	LLD	LLD	0.14	0.07	LLD	0.25
CaO	0.12	0.10	0.13	LLD	LLD	0.20	0.91	LLD	LLD	0.43	0.10	LLD	LLD
BaO	0.04	0.10	0.05	0.10	0.04	0.03	0.10	0.03	0.07	LLD	0.06	0.03	0.07
Na_2O	0.08	0.06	0.15	LLD	LLD	LLD	0.12	LLD	LLD	0.10	0.11	0.18	LLD
K_2O	LLD	LLD	LLD	LLD	LLD	LLD	LLD	LLD	LLD	LLD	LLD	LLD	LLD
Total	100.2	100.4	100.4	100.9	100.5	100.3	100.0	100.2	99.5	100.7	100.1	100.3	100.1
Mn/(Mn+Fe)	1.00	1.00	1.00	0.98	1.00	0.99	0.99	0.86	0.79	0.87	0.81	0.81	0.99

Abbreviations: N - number of analyses; LLD - lower than detection limit; n.a. - not analysed; Ptr-partridgeite; Bx-bixbyite; Hs-hausmannite; * $Mn_{(total)}$ expressed as Mn_2O_3; for hausmannite Mn^{2+}-Mn^{3+} charge balance calculated.

wt.%). Al_2O_3 concentrations range between 1.33 and 3.50 wt.%; Fe_2O_3, MgO and CaO contents are below 1 wt.% in the cryptomelane. The manganomelane of intermediate composition is characterized by variable concentrations of minor elements, containing 0.07–3.67 wt.% BaO, 1.12–1.58 wt.% Na_2O, 0.23–3.06 wt.% K_2O, 0.0–0.89 wt.% Fe_2O_3, and 1.21–2.01 wt.% Al_2O_3 (Table 4). Analytical totals of romanèchite, cryptomelane and manganomelane range between 93.3 and 97.2 wt.%, indicating the presence of variable amounts of absorbed and structural water (Frenzel, 1980).

Microprobe analyses of coarse grained pyrolusite indicated it to be essentially MnO_2, with negligible amounts of other elements (Table 4). The presence of absorbed water in the pyrolusite is indicated by analytical totals of between 97 and 98 wt.% (Frenzel, 1980).

Lithiophorite. De Villiers (1945*b*) described the occurrence of coarse botryoidal lithiophorite from the Glosam mine. A small piece of the original sample analysed by De Villiers (1945*b*) was used for microprobe analysis and atomic absorption spectrometry (Li_2O) (sample GLOLi01, Table 4) to compare its composition with that of the more abundant fine grained lithiophorite. Results compare very well, with Al_2O_3 and MnO_2 predominating and small amounts of Fe_2O_3, MgO (1.61 wt.% and 2.48 wt.%) and Li_2O (about 3 wt.%) present (Table 4). The results obtained in this study are also in very good agreement with the original analysis by De Villiers (1945*b*). The general formula $Li_2Mn^{2+}Mn_5^{4+}Al_4O_{18}{\cdot}6H_2O$ given by De Villiers (1945*b*) for the lithiophorite is thus essentially correct.

Gamagarite, apatite and baryte. Microprobe analyses of gamagarite were performed on a small piece of the type sample described by De Villiers (1943*b*). Results (Table 5) compare well with analyses by De Villiers (1943*b*) and Harlow *et al.* (1984), suggesting the formula $Ba_2(Fe^{3+},Mn)[(OH,H_2O)/(VO_4)_2]$. Apatite, present in the siliceous manganese ore, was found to have a hydroxy-apatite composition as no Cl or F were detected by microprobe analysis. The composition of baryte is fairly uniform, with 0–1.5 wt.% SrO substituting for BaO (Table 5).

Diaspore, ephesite, amesite and Ba-Al-muscovite. The presence of coarse grained ephesite, diaspore and amesite in the manganese ores has attracted the attention of several earlier workers (Chudoba, 1929; Hall, 1926; Coles-Phillips, 1931). Mn and Fe-bearing diaspore crystals, up to 10 cm long and with a distinct whisky brown to brownish red colour, were first described as rhodonite by Hall (1926) and later analysed by Chudoba (1929) who reported concentrations of 1.96 wt.% Fe_2O_3 and 4.32 wt.% Mn_2O_3. Nel (1929) found similar Fe_2O_3 concentrations of 1.32 to 1.47 wt.%, but detected only 0.11–0.5 wt.% Mn_2O_3. Electron microprobe analyses were performed to resolve the obvious disagreement between the results of these two studies (Table 5). Fe_2O_3 contents range between 0.3 and 0.54 wt.% and Mn_2O_3 contents between 0.2 and 0.6 wt.% (Table 5). Considerably larger Fe concentrations reported by Chudoba (1929) and Nel (1929) may be due to the presence of minute hematite inclusions in the diaspore crystals. Unit cell constants calculated for the diaspore from Guinier camera exposure of a single crystal fragment are $a = 4.401 \pm 0.002$ Å, $b = 9.428 \pm 0.002$ Å, $c = 2.845 \pm 0.001$ Å (D. Nyfeler, written communication 1994), in very good agreement with unit cell constants of diaspore reported in the ICDD (1994) database. X-ray and backscattered electron images of single crystal fragments oriented into different crystallographic orientations, indicated a homogenous distribution of Mn and Fe. It is suggested that the small amounts of $Fe^{3+}$and Mn^{3+} substitute for Al in the diaspore lattice. The presence of small amounts of Mn may also explain the unusual colour of the diaspore crystals.

Analyses of ephesite, the Na-rich analogue of margarite (Rösler, 1984) confirm the formula $(Na_{0.92}Li_{0.47})(Al_{2.04},Fe_{0.13},Mn_{0.14},Mg_{0.05})[(OH)_2/Al(Al_{0.92}Si_{0.08})Si_2O_{10}]$ (calculated for sample LOH176, Table 5). Amesite (Rösler, 1984), an aluminous serpentine mineral, has a composition (Table 5) of $Mg_{3.96}Al_{1.97}Mn^{2+}_{0.03}Fe^{3+}_{0.01}Ti_{0.01}[(OH)_8/(Si_{2.06},Al_{1.94})O_{10}]$ (sample BIS241) or $Mg_{3.87}Al_{1.95}Mn_{0.08}Fe_{0.03}[(OH)_8/(Si_{2.16}Al_{1.84})O_{10}]$ (sample GLO197). Ba-Al-muscovite, a mineral previously unknown in the PMF, was identified by microprobe analysis (Table 5) and has a composition corresponding to $(Ba_{0.6}K_{0.32}Na_{0.06}Mn^{2+}_{0.05}Fe^{2+}_{0.03})Al_{1.92}[(OH)_2/(Si_{2.44}Al_{1.56})O_{10}]$ if a stoichiometric water content is assumed.

Discussion

Origin and stability of ore-forming minerals. Members of the braunite group are known to be stable in various geological settings. Braunite and bixbyite form under metamorphic conditions ranging from lowest greenschist facies to granulite facies (Roy, 1981; Abs-Wurmbach *et al.*, 1983; Dasgupta and Manickavasagam, 1981). Several authors have presented convincing evidence for the early diagenetic formation of braunite as a reaction product of poorly crystalline Mn^{4+}-oxihydroxides and quartz (Ostwald and Bolton, 1990; Roy *et al.*, 1990; Ostwald, 1992). Others have advocated its sedimentary (Serdyuchenko, 1980; Hou, 1994) or even supergene origin (Ostwald, 1992). Partridgeite, or Fe-poor bixbyite, is only known from lower greenschist facies metamorphic assemblages (Roy

TABLE 4. Composition of manganese oxides of supergene origin (selected analyses, all data in wt.%)

Sample No.	DO171	LOH79	AUC198	GLO185	KAP229	BEE211	LOH179	GLO-Li01	LOH79	De Villiers	KAP229	DO169
Mineral	Crypt	Crypt	Mang	Mang	Rom	Rom	Rom	Lithio	Lithio	Lithio	Pyro	Pyro
N	6	5	5	3	3	5	3	5	3		5	3
SiO_2	0.52	0.88	0.40	1.12	0.20	0.34	0.45	LLD	LLD	0.30	0.78	2.28
TiO_2	0.12	0.02	0.06	0.07	LLD	LLD	0.03	0.41	0.20	n.a.	0.06	0.07
Al_2O_3	1.33	3.50	1.21	2.01	0.20	0.42	1.06	26.8	25.9	23.8	0.85	0.30
Fe_2O_3	LLD	0.93	0.89	LLD	0.07	0.65	0.35	0.63	2.16	0.96	LLD	LLD
MnO_2[a]	87.8	82.8	86.5	89.1	80.5	78.8	78.7	58.4	56.1	58.9	95.9	94.6
MgO	0.27	0.72	0.12	0.03	LLD	0.22	0.03	1.61	2.48	n.a.	LLD	LLD
CaO	0.17	LLD	0.20	0.84	LLD	0.10	0.23	0.02	0.20	LLD	LLD	0.20
BaO	0.43	1.99	3.67	0.07	15.4	13.3	15.7	0.10	0.07	n.a.	0.08	0.50
Na_2O	0.45	0.18	1.12	1.58	0.30	0.39	0.37	0.10	LLD	LLD	0.12	0.13
K_2O	5.42	4.92	3.06	0.23	LLD	0.86	LLD	LLD	0.10	LLD	LLD	0.10
Li_2O[b]	n.a.	n.a.	n.a.	n.a.	n.a.	n.a.	n.a.	3.31	n.a.	3.30	n.a.	n.a.
Total	96.5	96.0	97.2	95.0	96.7	95.1	96.9	88.2	87.3	100.2[c]	97.9	98.2

Abbreviations: N - number of analyses;
LLD - lower than detection limit;
n.a. - not analysed;
Crypt - cryptomelane;
Mang - manganomelane;
Rom - romanèchite;
Lithio - lithiophorite;
Pyro - pyrolusite;
[a] $Mn_{(total)}$ expressed as MnO_2; [b] Li_2O determined by atomic absorption spectroscopy (I. Finnegan, written comm.);
[c] includes 13.2 wt.% H_2O^+ and 1.45 wt.% H_2O^-.

TABLE 5. Composition of gangue minerals (selected analyses, all data in wt.%)

S. No.	Mn10-63	De Villiers	DO169	BEE211	GLO290	LOH293	BIS241	AUC202	BIS241	GLO197	GLO187	LOH176
Mineral	gamag	gamag	apatite	baryte	baryte	baryte	Mn-Di	Ba-Mu	amesite	amesite	ephesite	ephesite
N	5		8	5	5	5	10	5	5	5	3	3
SiO_2	0.17	n.a.	0.18	LLD	LLD	LLD	LLD	32.7	22.2	23.7	32.3	32.1
TiO_2	LLD	n.a.	0.06	n.a.	n.a.	n.a.	0.13	0.10	0.08	0.01	0.01	0.13
Al_2O_3	0.19	LLD	LLD	n.a.	n.a.	n.a.	84.2	39.6	35.7	35.3	52.1	52.6
Fe_2O_3	7.13	7.6	LLD	n.a.	n.a.	n.a.	0.54					
FeO								0.45	0.16	0.40	1.68	1.24
Mn_2O_3	5.93		0.67	n.a.	n.a.	n.a.	0.60					
MnO								0.89	0.42	1.07	1.60	1.33
MgO	0.11	5.5	LLD	LLD	LLD	LLD	0.10	0.22	26.6	28.5	0.34	0.24
CaO	LLD	n.a.	57.3	LLD	LLD	LLD	LLD	LLD	LLD	LLD	LLD	0.07
SrO	n.a.	n.a.	LLD	0.77	1.20	1.45	LLD	20.5	LLD	LLD	n.a.	n.a.
BaO	51.5	52.4	LLD	64.7	64.6	64.7	LLD	0.37	LLD	LLD	7.75	7.35
Na_2O	n.a.	n.a.	n.a.	n.a.	n.a.	n.a.	LLD	3.37	LLD	LLD	0.13	0.10
K_2O	n.a.	n.a.	n.a.	n.a.	n.a.	n.a.	<0.01	n.a.	n.a.	n.a.	n.a.	1.80
Li_2O[b]	n.a.	n.a.	n.a.	n.a.	n.a.	n.a.	14.6	n.a.	n.a.	n.a.	n.a.	n.a.
SO_3	LLD	n.a.	LLD	34.1	34.4	34.4	n.a.	n.a.	n.a.	n.a.	n.a.	n.a.
V_2O_5	32.1	31.9	n.a.	n.a.	n.a.	n.a.	n.a.	n.a.	n.a.	n.a.	n.a.	n.a.
P_2O_5	n.a.	n.a.	40.6	n.a.	n.a.	n.a.	n.a.	n.a.	n.a.	n.a.	n.a.	n.a.
Total	97.1	99.3[a]	98.8	98.8	99.0	99.1	100.2	98.2	85.1	89.0	95.9	97.0

Abbreviations: N - number of analyses;
LLD - lower than detection limit;
n.a. - not analysed;
Mn-Di - diaspore;
gamag - gamagarite;
Ba-Mu - barian-muscovite;
[a] includes 1.06 wt.% H_2O;
[b] Li_2O analysed by atomic absorption spectroscopy (I. Finnegan, written comm.).

et al., 1990; Gutzmer, 1996), although experimental studies suggest the stability of the association braunite–partridgeite at high temperatures and pressures of up to 600°C and 7 kbar at oxygen fugacities controlled by the MnO_2/Mn_2O_3 buffer (Abs-Wurmbach *et al.*, 1983). Apart from its occurrence in the Postmasburg manganese field, silica-depleted braunite has as yet only been recognized in the lower-greenschist facies metamorphic oxide ores of the Kajlidongri mine, India (Ostwald and Nayak, 1993), and as a major constituent of hydrothermally altered Wessels-type ore of the Kalahari manganese field (Kleyenstüber, 1985; Gutzmer and Beukes, 1995).

Braunite, silica-depleted braunite, braunite II, partridgeite and bixbyite from the Postmasburg manganese field occupy non overlapping fields in the SiO_2–Fe_2O_3 diagram (Fig. 9). The predominance of braunite in siliceous and partridgeite or bixbyite in the silica-poor ferruginous ores indicates that the distribution and composition of the different braunite group minerals in the manganese ores of the Postmasburg manganese field are controlled by the host rock composition.

Petrographic evidence suggests that braunite, partridgeite and Ca-poor silica-depleted braunite formed diagenetically in the manganese ores of the Postmasburg manganese field and were locally recrystallized during greenschist facies metamorphism. Very fine grained manganese ores preserved details of sedimentary and early diagenetic structures. Layered aggregates with fine fibrous botryoidal texture, now composed of braunite and partridgeite, closely resemble Mn^{4+}-oxihydroxide crusts described in Mesozoic unmetamorphosed karst-hosted wad deposits by Brannath and Smykatz-Kloss (1992). Concentric zonation in braunite was ascribed to diagenetic replacement processes by Ostwald (1982) and Plehwe-Leisen (1985). Replacement of authigenic quartz by braunite further supports a diagenetic origin for some of the braunite in the siliceous ores.

Sedimentary and early diagenetic textures are obscured in the more coarse grained manganese ores. Mosaic textures that are present in massive braunite-partridgeite ores are typical of metamorphosed manganese ores (Ramdohr, 1969; Roy, 1981). This suggests that recrystallization of early diagenetic braunite-partridgeite assemblages took place during metamorphism. The occurrence of bixbyite is restricted to isolated pods of very coarsely recrystallized ferruginous manganese ores. Textures such as veining, brecciation and the abundance of vugs indicate that bixbyite-rich ores formed as a result of localized metasomatism, with hydrothermal fluids most probably expelled from immediate host rocks.

The coexistence of pyrophyllite and diaspore in the aluminous shales of the Gamagara Formation suggests formation from kaolinitic clays at temperatures between 300 and 350°C (Anovitz *et al.*, 1991) and a pressure of 3 to 4 kbar (Fig. 8). The crystallinity of illite in the Gamagara shales confirms greenschist facies metamorphic conditions with peak metamorphic temperatures below 400°C (Plehwe-Leisen, 1985). Nell *et al.* (1994) showed that the bixbyite in the ferruginous manganese ore formed in a temperature range of between 315 to 375°C, i.e. during peak metamorphism. Diaspore, ephesite and amesite are known to be stable under greenschist facies metamorphism (Bárdossy, 1982; Feenstra, 1996; Anovitz *et al.*, 1991). Acmite has recently been reported as a minor constituent of the greenschist facies manganese-rich iron-formations of the Cuyuna Range, USA (McSwiggen *et al.*, 1994).

Meteoric fluids are thought to be responsible for the replacement of the greenschist facies manganese ore mineral assemblage. The abundance of roma-

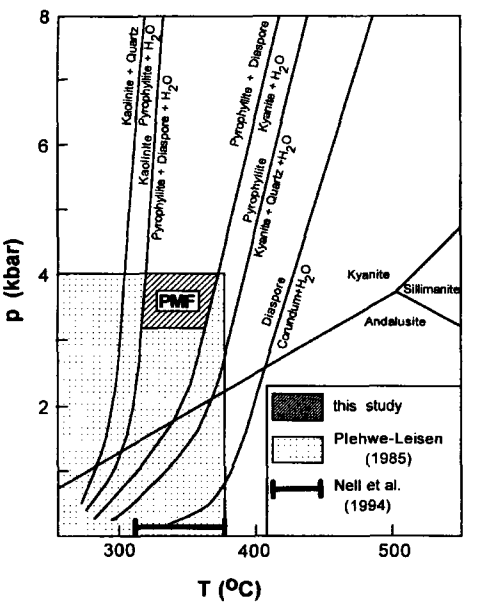

FIG. 8. Stable equilibria in the system Al_2O_3-SiO_2-H_2O (Anovitz *et al.*, 1991). Hatched area outlines peak metamorphic conditions suggested for the manganese ores and associated sediments of the Olifantshoek Group in the Postmasburg manganese field. Lower greenschist metamorphic conditions are in agreement with the temperature of formation of bixbyite (Nell *et al.*, 1994) and metamorphic conditions estimated by Plehwe-Leisen (1985) for the Postmasburg manganese field.

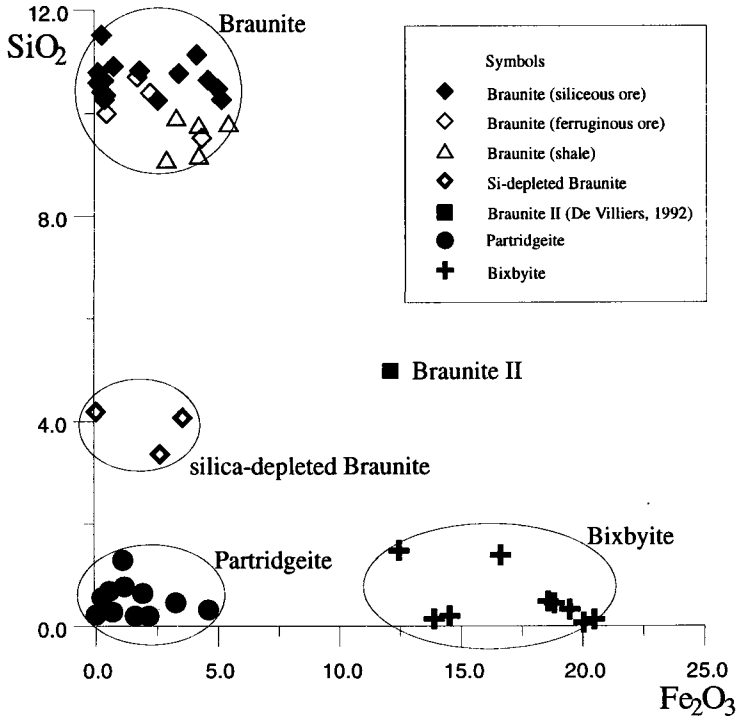

FIG. 9. SiO_2–Fe_2O_3 diagram to discriminate different members of the braunite-bixbyite group of minerals. Note clear separation between partridgeite and braunite.

nèchite and cryptomelane indicates that considerable amounts of barium and potassium were introduced during supergene alteration.

The crystal chemistry of the braunite group. The crystal chemistry of three of the members of the braunite group present in the Postmasburg manganese field, namely braunite, braunite II and bixbyite, can be explained by the polysomatic stacking model of De Villiers and Buseck (1989). This model envisages stacking of layer modules of braunite $Mn_2^{2+}Mn_7^{3+}SiO_{24}$, bixbyite $(Mn,Fe)_{16}O_{24}$, and braunite II $CaMn_{14}^{3+}SiO_{24}$. However, the chemical composition of the other two minerals of the braunite group, namely partridgeite and Ca-poor silica-depleted braunite, cannot be explained without adding a partridgeite layer module to the existing model. The partridgeite module, expressed as $Mn_{16}O_{24}$, most probably has lower symmetry than the Fe-rich bixbyite module, as is indicated by the optical anisotropy of partridgeite in the manganese ore. Partridgeite in the Postmasburg manganese field is thought to be essentially composed of this new module. The composition of Ca-poor silica-depleted braunite could then be explained by stacking three layers of the partridgeite module with two layers of the braunite module.

Iron is apparently fractionated into braunite in cogenetic braunite-partridgeite pairs (Fig. 10A) but into bixbyite in braunite-bixbyite pairs (Fig. 9) (Dasgupta *et al.*, 1990). The observed reversal in the fractionation is at present not fully understood but may be related to the stabilization of bixbyite (Fe-rich α-Mn_2O_3) at decreasing metamorphic oxygen fugacities by increasing substitution of Fe for Mn (Abs-Wurmbach *et al.*, 1983).

Differences in the minor element composition of braunite, partridgeite, bixbyite, Ca-poor silica-depleted braunite and braunite II reflect small differences in their crystal chemical properties. The enrichment of TiO_2 in shale-hosted braunite is related to the presence of a tetrahedrally coordinated site, occupied by Si, in the braunite layer module (Fig. 10B). The presence of unusually high concentrations of CaO in braunite II (Fig. 10C) reflects the presence of a distinct Ca-bearing module in the structure of braunite II (De Villiers and Buseck, 1989). The CaO concentrations in braunite and Ca-poor silica-depleted braunite are lower than in

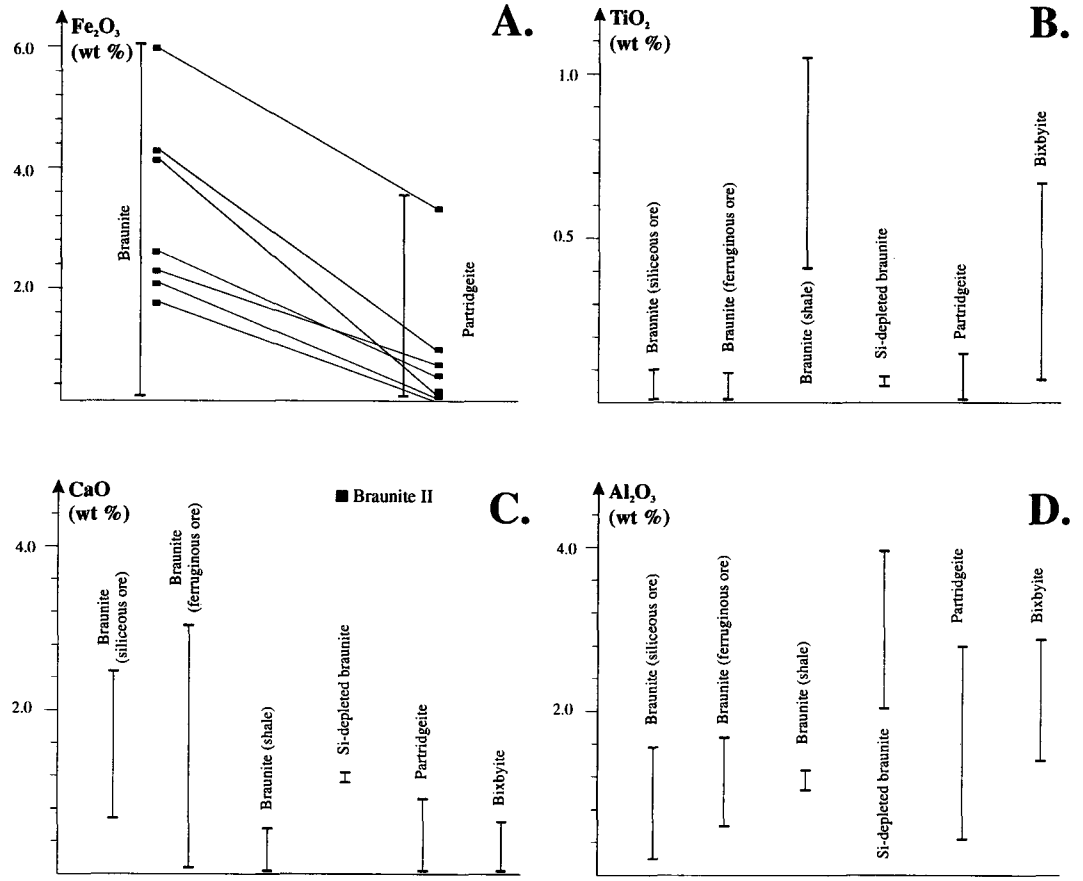

FIG. 10. (A) Fe_2O_3 content of braunite and partridgeite. Coexisting pairs are connected by tie lines. Ranges of the contents of TiO_2 (B), CaO (C) and Al_2O_3 (D) in the different members of the braunite-bixbyite group of minerals.

braunite II but considerably larger than those in partridgeite and bixbyite (Fig. 10C), suggesting substitution of Ca for Mn^{2+} in braunite group minerals (Baudracco-Gritti, 1985; Abs-Wurmbach *et al.*, 1983). Al_2O_3 concentrations (Fig. 10D) are greatest in silica-depleted braunite. Al_2O_3 contents in bixbyite and partridgeite are below those in Ca-poor silica-depleted braunite but much larger than in braunite (Fig. 10D). The fractionation of aluminium into Ca-poor silica-depleted braunite needs further investigation since Al^{3+} apparently substitutes for Mn^{3+} and not Si^{4+} in the braunite group of minerals (Abs-Wurmbach and Langer, 1975).

Conclusions

The manganese ores of the Postmasburg manganese field were apparently derived from a manganese wad precursor in a karstic setting under diagenetic to low-grade metamorphic conditions. The peak metamorphic temperature was not greater than 375°C at 3–4 kbar pressure. The metamorphic oxide assemblage reflects a regionally uniform lower greenschist facies metamorphic overprint for the entire deposit, unlike suggested by Schneiderhöhn (1931), De Villiers (1960) and De Villiers (1983).

Five members of the braunite group are present in the Postmasburg manganese ores, namely braunite, braunite II, Ca-poor silica-depleted braunite, partridgeite and bixbyite. Iron-poor partridgeite is a distinct phase that is chemically and optically easily distinguished from Fe-rich bixbyite. The phase chemistry of braunite, braunite II and bixbyite is in agreement with the polysomatic stacking model for the braunite group proposed by De Villiers and Buseck (1989). However, the composition of partridgeite and Ca-poor silica-depleted braunite can only be explained in terms of this polysomatic

stacking model if a module layer with a partridgeite composition, $Mn_{16}O_{24}$, is introduced.

Acknowledgements

The authors are greatly indebted to the geological staff of ASSMANG (Beeshoek), ISCOR (Sishen), SAMANCOR (Hotazel) and Rio Tinto Exploration for their permission to visit their properties in the Postmasburg manganese field. Special thanks to Willem Grobbelaar, Technical Manager at Beeshoek Iron Ore Mine, for logistical support and many interesting discussions during field work in 1993 and 1994 by J.G. We want to express special thanks to Andreas 'Hasselblad'-Pack, for his expert advice on how to obtain high quality black and white photomicrographs and to Daniel Nyfeler (Bern) for information on the manganese-bearing diaspore. We are also grateful to J. Ostwald whose thorough review helped to improve the quality of the final manuscript.

References

Abs-Wurmbach, I. and Langer, K. (1975) Synthetic Mn^{3+}-kyanite and viridine $(Al_{2-x}Mn^{3+}_x)SiO_5$, in the system Al_2O_3-MnO_2-SiO_2. *Contrib. Mineral. Petrol.*, **49**, 21–38.

Abs-Wurmbach, I., Peters, Tj., Langer, K. and Schreyer, W. (1983) Phase relations in the system Mn-Si-O and experimental and petrological study. *Neues Jahrb. Mineral. Abh.*, **146**, 258–79.

Afifi, A.M. and Essene, E.J. (1988) Minfile Version 3-88 (software package).

Anovitz, L.M., Perkins, D. and Essene, E.J. (1991) Metastability in near-surface rocks of minerals in the system Al_2O_3-SiO_2-H_2O. *Clays Clay Miner.*, **39**, 225–33.

Bárdossy, G. (1982) *Karst Bauxites - Bauxite Deposits on Carbonate Rocks.* Elsevier, Amsterdam, 441 pp.

Baudracco-Gritti, C. (1985) Substitution du manganese bivalent par du calcium dans les minéraux du groupe: Braunite, neltnerite, braunite II. *Bulletin de Minéralogie*, **108**, 437–45.

Beukes, N.J. (1986) The Transvaal Sequence in Griqualand West. In *Mineral Deposits of Southern Africa* (C.R. Annhaeusser and S. Maske, eds.). Geol. Soc. S. Afr., Johannesburg, **1**, 819–28.

Beukes, N.J. and Smit, C.A. (1987) New evidence for thrust faulting in Griqualand West, South Africa: Implications for stratigraphy and the age of red beds. *Trans. Geol. Soc. S. Afr.*, **90**, 378–94.

Brannath, A. and Smykatz-Kloss, W. (1992) Mineralogische Untersuchungen an einigen hessischen Mangan-Eisenerzvorkommen. *Chemie der Erde*, **52** 3–31.

Coles-Phillips, F.C. (1931) Ephesite (soda-margarite) from the Postmasburg district, South Africa. *Mineral. Mag.*, **22**, 482–5.

Chudoba, K. (1929) Über 'Mangandiaspor' und Manganophyll von Postmasburg (Griqualand West, Südafrika). *Neues Jahrb. Mineral., Beilagen Band 64 A*, 11–8.

Dasgupta, H.C. and Manickavasagam, R. (1981) Chemical and X-ray investigation of braunite from the metamorphosed manganiferous sediments of India. *Neues Jahrb. Mineral. Abh.*, **142, 2**, 149–60.

Dasgupta, S., Bannerjee, U., Fukuoka, M., Bhattacharya, P.K. and Roy, S. (1990) Petrogenesis of metamorphosed manganese deposits and the nature of the precursor sediments. *Ore Geol. Rev.*, **5**, 359–84.

De Villiers, J. (1960) *Manganese Deposits of the Union of South Africa.* Geol. Surv. S. Afr., Pretoria, 280 pp.

De Villiers, J.E. (1943*a*) A preliminary description of the new mineral partridgeite. *Amer. Mineral.*, **28**, 336–8.

De Villiers, J.E. (1943*b*) Gamagarite, a new vanadium mineral from the Postmasburg manganese deposits. *Amer. Mineral.*, **28**, 329–35.

De Villiers, J.E. (1945*a*) Some minerals occurring in South African manganese deposits. *Trans. Geol. Soc. S. Afr.*, **48**, 17–25.

De Villiers, J.E. (1945*b*) Lithiophorite from the Postmasburg manganese deposits. *Amer. Mineral.*, **30**, 629–34.

De Villiers, J.E. (1983) The manganese deposits of Griqualand West, South Africa: Some mineralogic aspects. *Econ. Geol.*, **78**, 1108–18.

De Villiers, J.E. (1992) On the origin of the Griqualand West manganese and iron deposits. *S. Afr. J. Sci.*, **88**, 12–5.

De Villiers, J.P.R. and Buseck, P.R. (1989) Stacking variations and nonstoichiometry in the bixbyite-braunite polysomatic mineral group. *Amer. Mineral.*, **74**, 1325–36.

De Villiers, P.R. and Herbstein, F.H. (1967) Distinction between two members of the braunite group. *Amer. Mineral.*, **52**, 20–30.

Feenstra, A. (1996) An EMP and TEM-AEM study of margarite, muscovite and paragonite in polymetamorphic metabauxites of Naxos (Cyclades, Greece) and the implications of fine-scale mica interlayering and multiple mica generations. *J. Petrol.*, **37**, 201–33.

Frenzel, G. (1980) The manganese ore minerals. In *Geology and Geochemistry of Manganese* (I.M. Varentsov and Gy. Grasselly, eds.). Schweizerbartsche Verlagsbuchhandlung, Stuttgart, **1**, 25–157.

Grobbelaar, W.S. and Beukes, N.J. (1986) The Bishop and Glosam manganese mines and Beeshoek iron ore mine of the Postmasburg area. In *Mineral Deposits of Southern Africa* (C.R. Annhaeusser and S. Maske, eds.). Geol. Soc. S. Afr., Johannesburg, **1**, 957–61.

Gutzmer, J. (1996). *Genesis and alteration of the*

Kalahari and Postmasburg manganese deposits, Griqualand West. South Africa. PhD thesis (unpubl.), RAU, Johannesburg, 513 pp.

Gutzmer, J. and Beukes, N.J. (1995). Fault-controlled metasomatic alteration of Early Proterozoic sedimentary manganese ores in the Kalahari manganese field, South Africa. *Econ. Geol.*, **90**, 823–44.

Hall, A.L. (1926) The manganese deposits near Postmasburg, West of Kimberley. *Trans. Geol. Soc. S. Afr.*, **29**, 17–66.

Harlow, G.E., Dunn, P.J. and Rossman, G.R. (1984) Gamagarite: A reexamination and comparison with brackebuschite-like minerals. *Amer. Mineral.*, **69**, 803–6.

Hou, B. (1994) Primary braunite in Triassic sedimentary manganese deposits of Dounan, Yunnan, China. *Ore Geol. Rev.*, **9**, 219–39.

Kleyenstüber, A.S.E.(1985) *A regional mineralogical study of the manganese-bearing Voëlwater Subgroup in the Northern Cape Province.* PhD thesis (unpubl.), RAU, Johannesburg, 328 pp.

Mason, B. (1944) The system Mn_2O_3-Fe_2O_3: Some comments on the names bixbyite, sitaparite and partridgeite. *Amer. Mineral.*, **29**, 66–9.

McSwiggen, P.L., Morey, G.B. and Cleland, J.M. (1994) The origin of aegirine in iron formation of the Cuyuna Range East Central Minnesota. *Canad. Mineral.*, **32**, 589–98.

Nel, L.T. (1929) *The geology of the Postmasburg manganese deposits and the surrounding country. Explanation of the geological map.* Geol. Surv. S. Afr., Pretoria, 109 pp.

Nell, J., Pollak, H. and Lodya, J.A. (1994) Intersite cation partitioning in natural and synthetic alpha-$(Fe,Mn)_2O_3$ (bixbyite) solid solutions determined from ^{57}Fe Mössbauer spectroscopy. *Hyperfine Interactions*, **91**, 601–5.

Ostwald, J. (1982) Some observations on the mineralogy and genesis of braunite. *Mineral. Mag.*, **46**, 506–7.

Ostwald, J. (1992) Diagenetic and supergene braunites in the Proterozoic Manganese Group, Western Australia. *Mineral. Mag.*, **56**, 611–6.

Ostwald, J. and Bolton, B.R. (1990) Diagenetic braunite in sedimentary rocks of the Proterozoic Manganese Group, Western Australia. *Ore Geol. Rev.*, **5**, 315–23.

Ostwald, J. and Nayak, V.K. (1993) Braunite mineralogy and paragenesis from the Kajlidongri mine, Madhya Pradesh, India. *Mineral. Depos.*, **28**, 153–6.

Plehwe-Leisen, E. von (1985) *Geologische und erzpetrographische Untersuchungen der Manganerze des Postmasburgfeldes, Nördliche Kapprovinz, Südafrika.* Dissertation (unpubl.), Ludwig-Maximilians Universität München, Munich, 129 pp.

Ramdohr, P. (1969) *The Ore Minerals and their Intergrowths.* Pergamon Press, Oxford, 1174 pp.

Ramdohr, P. and Frenzel, G. (1956) Die Manganerze. In *Symposium Sobre Yacimientos de Manganeso, Mexico City* (J.G. Reyna, ed.), 19–73.

Rösler, H.J. (1984) *Lehrbuch der Mineralogie* (third edition). VEB Verlag, Leipzig, 833 pp.

Roy, S. (1981) *Manganese Deposits.* Academic Press, London, 458 pp.

Roy, S., Bandopadhyay, P.C., Perseil, E.A. and Fukuoka, M. (1990) Late diagenetic changes in manganese ores of the Upper Proterozoic Penganga Group, India. *Ore Geol. Rev.*, **5**, 341–57.

Schneiderhöhn, H. (1931) Mineralbestand und Gefüge der Manganerze von Postmasburg, Griqualand West, Südafrika. *Neues Jahrb. Mineral., Beilagen Band* **64 A**, 701–26.

Serdyuchenko, D.P. (1980) Precambrian biogenic-sedimentary manganese deposits. In *Geology and Geochemistry of Manganese* (I.M. Varentsov and G. Grasselly, eds.). Schweizerbartsche Verlagsbuchhandlung, Stuttgart, **2**, 61–88.

Van Schalkwyk, J.F. and Beukes, N.J.(1986) The Sishen iron ore deposit, Griqualand West. In *Mineral Deposits of Southern Africa* (C.R. Annhaeusser and S. Maske, eds.). Geol. Soc. S. Afr., Johannesburg, **I**, 931–56.

Van Wyk, J.P. (1980) *Die geologie van die gebied Rooinekke-Matsap-Wolhaarkop in Noord-Kaapland met spesiale verwysing na die Koegas-Subgroep, Transvaal-Supergroep.* MSc thesis (unpubl.), RAU, 159 pp.

Van Wyk, J.P. and Beukes, N.J. (1982) The geology of the Sishen iron ore deposit. In *Proceedings. 12th CMMI Congress* (H.W. Glen, ed.). Geol. Soc. S. Afr., Johannesburg, 203–11.

[*Manuscript received 28 May 1996: revised 29 August 1996*]